

Plasmon–exciton induced transparency in plexcitonic Ag–CuCl-coated nanowires and associated arrays

ShuMin Jiang¹ · QiuYue Xie² · DaJian Wu²

Received: 1 December 2014 / Accepted: 11 March 2015 / Published online: 20 March 2015
© Springer-Verlag Berlin Heidelberg 2015

Abstract The plasmon–exciton couplings in Ag–CuCl-coated nanowires (ACNWs) have been investigated by using the scattering theory and the finite element method. It is found with increasing the shell thickness that the dipole plasmon resonance of the Ag nanowire can be tuned through the exciton resonance in the CuCl shell. The strong coupling between the plasmon resonance in the Ag nanowire and the exciton resonance in the CuCl shell leads to two new hybridized plexcitonic modes. The dispersion curves of the plexcitonic modes in the ACNWs are studied, and the obtained splitting energy is about 88 meV. We further find that the destructive interference between the plasmon and exciton resonances results in the plasmon–exciton induced transparency. As the TE wave propagates through the ACNW array, an extraordinary transmittance can be found in the ACNW array at the scattering dip of the ACNW.

1 Introduction

Metal–semiconductor hybrid nanostructures have received increasing attention over the past few years because of their promising applications in optical sensing, light emitter, photovoltaic system, and quantum information [1–6]. The surface plasmons (SPs) in metal nanostructures can interact with the excitons in semiconductor nanostructures

when they are in close proximity [5, 7]. The weak couplings between the plasmon and exciton resonances can lead to the induced transparency, enhanced absorption, increased emission, and increased optical nonlinearity [4, 8–13]. The strong plasmon–exciton couplings will modify the responses of the plasmon and exciton modes. J aggregates can strongly couple with the surface plasmon polariton [14–16] or the localized surface plasmon resonance (LSPR) [17, 18] leading to new hybridized plasmon–exciton states (plexcitons). The dispersion curves of two plexcitonic modes show an avoided crossing, which is known as Rabi splitting [5]. Fofang et al. [19, 20] further reported the enhanced and tunable nonlinear optical properties in the Au nanoshell–J aggregate complexes. As a quantum emitter (QE) locates at the center of a dimer nanoantenna, a Rabi splitting has been found in the scattering spectrum [21]. It was also found that the interaction between the quantum emitter and the gap plasmon can result in a Fano resonance in the metallic dimer–QE system [22]. In addition, Marinica et al. [23] found that the electron transfer of the excited electron into the metal can decrease the lifetime of the exciton in the QE.

Recently, Manassah [24] investigated the electrodynamics of CuCl-coated Ag nanoshells. Semiconductor CuCl exhibits a strong Z_3 exciton line at about 3.202 eV [7, 25]. The plasmon–exciton couplings in the Ag–CuCl nanoshell lead to a splitting of the excitonic line and a shift in LSPR. In the dimer including a CuCl nanosphere and an Ag nanosphere, the exciton resonances of the CuCl nanosphere interact with the SP resonances of the Ag nanoparticles resulting in the induced transparency and slow light effect [8]. We also found that the plasmon–exciton couplings in the Ag nanoshell with a semiconductor CuCl core can lead to the Rabi splitting and the induced transparency by changing the geometry of the CuCl–Ag nanoshell [26]. To

✉ DaJian Wu
wudajian@njnu.edu.cn

¹ Faculty of Science, Jiangsu University, Zhenjiang 212013, China

² Jiangsu Key Lab on Opto-Electronic Technology, School of Physics and Technology, Nanjing Normal University, Nanjing 210023, China

our knowledge, little work has been carried out on the plasmon–exciton couplings in the plexcitonic nanowires [27–29], especially on the associated arrays.

In this paper, we investigate the plasmon–exciton couplings in an Ag nanowire coated with a CuCl outer shell (ACNW) by means of the scattering theory. The strong coupling between the LSPR in the Ag nanowire and the exciton resonance in the CuCl shell leads to two new hybridized plexcitonic modes. The dispersion curves of the plexcitonic modes in the ACNWs have been studied. It is found that the destructive interference between the $\omega_{\text{Ag}|1}$ and ω_e modes can result in the plasmon–exciton induced transparency. Furthermore, we investigate the transmission properties of the TE wave propagating through the ACNW arrays by using the finite element method (FEM).

2 Electromagnetic scattering model

The TE wave propagating through the ACNW array is shown in Fig. 1. The ACNW comprises an Ag nanowire with radius r_1 and an outer CuCl shell with thickness $(r_2 - r_1)$. The gap between the two ACNWs is defined as d . The ACNW is infinitely long. The propagation and polarization vectors of the TE wave are parallel to y axis and x axis, respectively. The dielectric function of the Ag nanowire ε_1 has real and imaginary frequency-dependent components and can be expressed as [30]

$$\varepsilon_1(\omega) = 1 - \frac{\omega_p^2}{\omega^2 + i\omega\gamma_f} + \chi_\infty \quad (1)$$

where the background susceptibility χ_∞ is about 4, the bulk plasma frequency $\hbar\omega_p = 8.9780$ eV, and the bulk collision frequency $\hbar\gamma_f = 0.0212$ eV. The dielectric function of the CuCl shell ε_2 can be expressed as [24, 31]

$$\varepsilon_2(\omega) = \varepsilon_\infty + 3\pi\eta \frac{\gamma}{\omega_0 - \omega - i\gamma} \quad (2)$$

where ε_∞ is the background dielectric function and η is the scaled atomic average density $\lambda^3 N/V$. The reduced resonance wavelength λ is defined as c/ω_0 . The decay rate $\gamma/2\pi$ arises from the Z_3 exciton line width. For CuCl shell, $\varepsilon_\infty = 5.59$, the exciton resonance frequency $\hbar\omega_0 = 3.3022$ eV, the loss factor $\hbar\gamma = 4.9206 \times 10^{-5}$ eV, and $3\pi\eta = \varepsilon_\infty \hbar\Delta_{\text{LT}}/\hbar\gamma = 632$ corresponds to the exciton oscillator strength. Here, $\hbar\Delta_{\text{LT}} = 5.65$ meV is the exciton longitudinal transverse splitting. We assume that the ACNWs are embedded in vacuum with $\varepsilon_3 = 1$.

The incident light interacting with an infinite ACNW can be described by the scattering theory [32]. The electromagnetic waves are expanded by using vector cylindrical harmonic functions, and then, Maxwell's boundary conditions

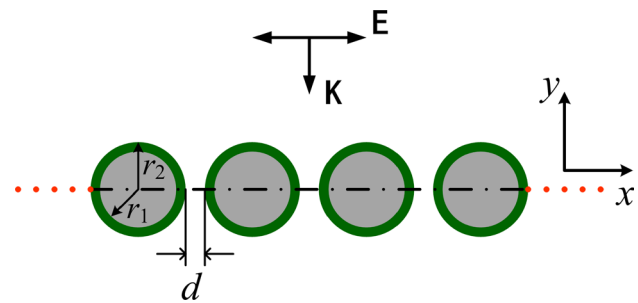


Fig. 1 Schematic diagram for TE wave propagating through the ACNW array

are applied to resolve the unknown expansion coefficients of the scattered and interior waves. For TE wave, the scattering efficiency $Q_{\text{sca},l}$ can be expressed as [32]

$$Q_{\text{sca},l} = \frac{2}{kr_2} \left[|a_{0l}|^2 + 2 \sum_{n=1}^{\infty} (|b_{nl}|^2 + |a_{nl}|^2) \right] \quad (3)$$

where a_{nl} and b_{nl} are the scattering coefficients. a_{0l} and a_{1l} correspond to the magnetic (MD) and electric (ED) dipole modes, respectively [33]. The TE wave propagating through the ACNW array can be studied by using the 2D-FEM [34]. The FEM has been proved to be an efficient numerical tool to investigate the optical properties of the metallic nanostructures [35–37]. We calculate the scattering parameters S_{11} and S_{21} of the ACNW array. Scattering parameters originate from transmission-line theory. In our model, the incident and transmission ports are defined as ports 1 and 2, respectively. S_{11} is the reflection coefficient at port 1, and S_{21} is the transmission coefficient from port 1 to port 2. The time average power reflection and transmission coefficients can be obtained as $R = |S_{11}|^2$ and $T = |S_{21}|^2$, respectively.

3 Results and discussion

We firstly investigate the scattering properties of the ACNWs. In Fig. 2a, the solid and dashed lines show the scattering spectra of an Ag nanowire and a CuCl nanotube, respectively. The radius of the Ag nanowire is fixed at 20 nm. For the CuCl nanotube, r_1 and r_2 are fixed at 20 and 25 nm, respectively, and ε_1 is fixed at 1. A broad peak appears at about 3.2675 eV in the scattering spectrum of the Ag nanowire, which is due to the dipole plasmon resonance. A very sharp exciton peak can be found at about 3.3040 eV in the scattering spectrum of the CuCl nanotube. Figure 2b shows the scattering spectrum of the ACNW. Here, r_1 and r_2 are fixed at 20 and 25 nm, respectively. Figure 2c, d represents the contributions from the

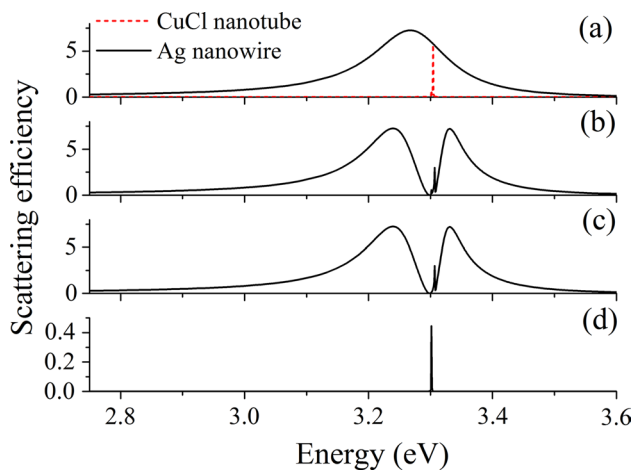


Fig. 2 **a** Scattering spectra of an Ag nanowire and a CuCl nanotube. **b** Scattering spectrum of the ACNW with $r_1 = 20$ nm and $r_2 = 25$ nm. Contributions from **c** the electric dipole mode and **d** the magnetic dipole mode

ED and MD resonances, respectively. The weak peak at about 3.3015 eV corresponds to the MD resonance in the ACNW, which arises from the high real part of the permittivity of CuCl. The high-permittivity nanowires have been reported to support the artificial magnetic resonances [33]. In the scattering spectrum of the ED mode, the peaks at about 3.3307 and 3.2394 eV correspond to the high- and low-energy plexcitonic modes, respectively. Compared with the plasmon resonance in the Ag nanowire and the exciton resonance in the CuCl nanotube, we can confirm that the strong coupling between the plasmon and exciton resonances occurs in the ACNW. In the ACNW, the strong coupling between the dipole plasmon resonance in the Ag nanowire ($\omega_{\text{Ag}|1}$) and the exciton resonance (ω_e) in the CuCl shell results in two new plexcitonic modes. The high-energy mode ($\omega_{\text{Ag}|1}^e|_1^h$) and low-energy mode ($\omega_{\text{Ag}|1}^e|_1^l$) correspond to the antibonding and bonding between the $\omega_{\text{Ag}|1}$ and ω_e modes, respectively [18, 19]. A scattering dip can be observed at about 3.2988 eV, which results from the destructive interference between the $\omega_{\text{Ag}|1}$ and ω_e modes [18, 21]. We also note that a weak peak appears at about 3.3067 eV. It is found with increasing the CuCl shell thickness that this peak always locates at about 3.3067 eV, but the strength of this peak is increased, as shown in Fig. 3. We think that this peak may arise from the interband transition, which corresponds to the bare exciton transition with frequency of ω_0 .

Figure 3 shows the scattering spectra of the ACNWs with r_2 of (a) 21, (b) 23, (c) 25, (d) 27, and (e) 29 nm. Here, r_1 is fixed at 20 nm. In Fig. 3a, a strong peak appears at about 3.5247 eV and a sharp peak appears at about 3.2997 eV. The peaks at about 3.5247 and 3.2997 eV represent the $\omega_{\text{Ag}|1}$ mode in the Ag nanowire and the ω_e mode in

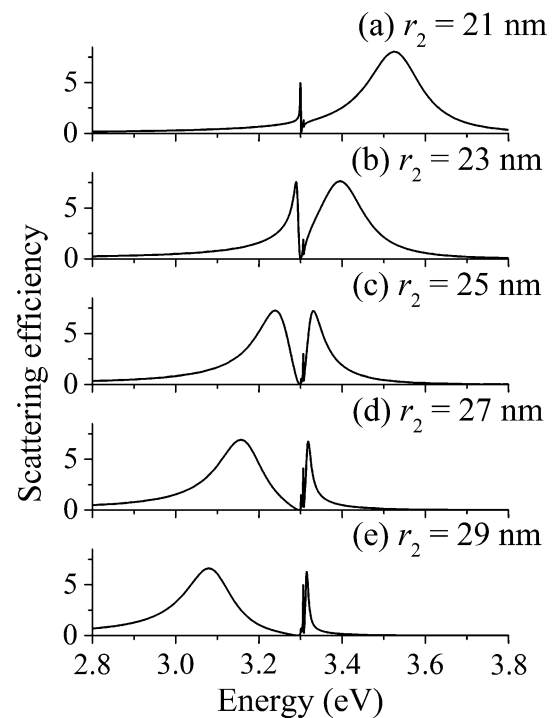


Fig. 3 Scattering spectra of the ACNWs with r_2 of **a** 21, **b** 23, **c** 25, **d** 27, and **e** 29 nm. Here, r_1 is fixed at 20 nm

the CuCl shell, respectively. In this case, the line width of the ω_e mode is much smaller than that of the $\omega_{\text{Ag}|1}$ mode. The sharp ω_e peak interferes with the broad $\omega_{\text{Ag}|1}$ peak leading to a Fano resonance in the scattering spectrum. The Fano resonances due to the plasmon–exciton couplings have been widely reported in many previous papers [18, 19, 21]. Therefore, an asymmetric Fano peak can be observed at about 3.2997 eV. In Fig. 3b, the increased thickness of the CuCl shell leads to the redshift of the LSPR peak. The increased thickness of the CuCl shell decreases the oscillation strength of the conduction electrons in the Ag nanowire, and hence, the energy of the $\omega_{\text{Ag}|1}$ mode decreases. Thus, the $\omega_{\text{Ag}|1}$ peak can be tuned through the exciton resonance of the CuCl shell with increasing r_2 values. Meanwhile, the increased thickness of the CuCl shell also will enhance the strength of the exciton peak. However, in Fig. 3b, the line width of the ω_e peak is still much smaller than that of $\omega_{\text{Ag}|1}$ peak. The interference between the $\omega_{\text{Ag}|1}$ and ω_e peaks leads to a Fano resonance in the scattering spectrum of the ACNW. As r_2 increases to 25 nm, a true Rabi splitting can be found in Fig. 3c. The peaks at about 3.3307 and 3.2394 eV correspond to the $\omega_{\text{Ag}|1}^e|_1^h$ and $\omega_{\text{Ag}|1}^e|_1^l$ modes, respectively. A transparency dip also can be observed in the scattering spectrum at about 3.2988 eV, which results from the destructive interference between the $\omega_{\text{Ag}|1}$ and ω_e modes. In Fig. 3d, e, with further increases in the r_2 value, the $\omega_{\text{Ag}|1}^e|_1^h$ and $\omega_{\text{Ag}|1}^e|_1^l$ peaks both redshift

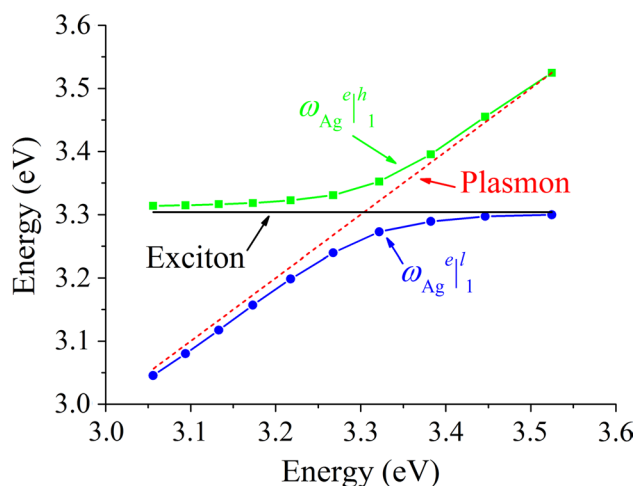


Fig. 4 Dispersion curves of the plexcitonic modes in the ACNWs. Here, r_1 is fixed at 20 nm

and the separation between the two peaks increases. As $r_2 \geq 25$ nm, the MD mode can be found in the scattering spectra because of the large thickness of the CuCl shell.

It was found with increasing the CuCl shell thickness that the $\omega_{\text{Ag}}^e|l|_1$ peak of the Ag nanowire can be tuned through the ω_e peak of the CuCl shell. Therefore, we can carefully study the coherent coupling energy in the ACNW. Figure 4 shows the dispersion curves of two plexcitonic modes in the ACNWs. Here, r_1 is fixed at 20 nm. The dashed-square line shows the resonance energy of the $\omega_{\text{Ag}}^e|h|_1$ mode, while the dashed-circle line represents the resonance energy of the $\omega_{\text{Ag}}^e|l|_1$ mode. The solid and dashed lines show the resonance energies of the uncoupled exciton and plasmon modes, respectively. We can find an avoided crossing in the dispersion curves. The Rabi splitting energy is calculated to be about 88 meV, which indicates the strength of the plasmon–exciton coupling in the ACNW. The Rabi splitting energies in different plasmon–exciton complexes can change from a few millielectron volts to several hundreds of millielectron volts [17–19, 21, 38]. The small Rabi splitting energy in the ACNW is due to the narrow exciton line and the large dielectric constant of CuCl. Some previous reports have carefully investigated the transition from Fano resonance to Rabi splitting [18, 21]. It is known that the Rabi splitting occurs when the coupling energy is larger than $(\gamma_{\text{LSPR}} - \gamma_0)/2$ [18]. Here, γ_{LSPR} and γ_0 are the relative resonance line widths of the LSPR and exciton modes, respectively. Based on the above calculations, we can confirm that the ACNW can satisfy this criterion, as $(\gamma_{\text{LSPR}} - \gamma_0)/2 \approx 75$ meV.

Figure 5a shows the scattering spectrum of the ACNW with $r_1 = 20$ nm and $r_2 = 25$ nm, which was calculated by using the 2D-FEM. This scattering spectrum matches well with that obtained by using the scattering theory.

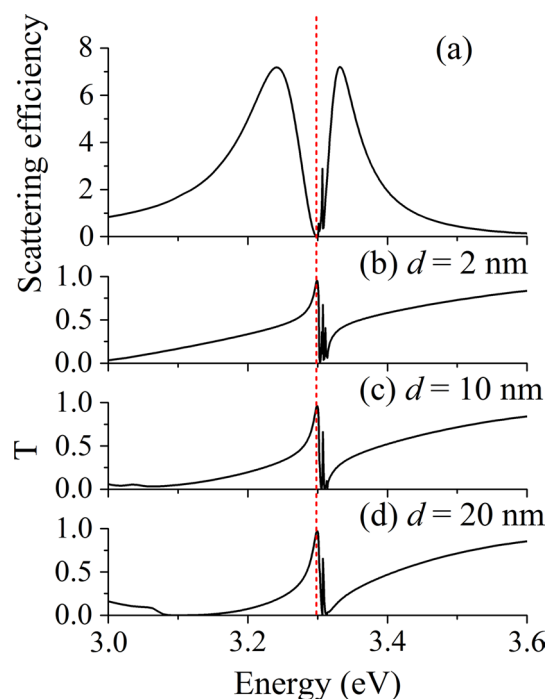


Fig. 5 a Scattering spectrum of the ACNW with $r_1 = 20$ nm and $r_2 = 25$ nm. Transmission spectra of the ACNW arrays with b $d = 2$ nm, c $d = 10$ nm, and d $d = 20$ nm. Here, r_1 and r_2 are fixed at 20 and 25 nm, respectively

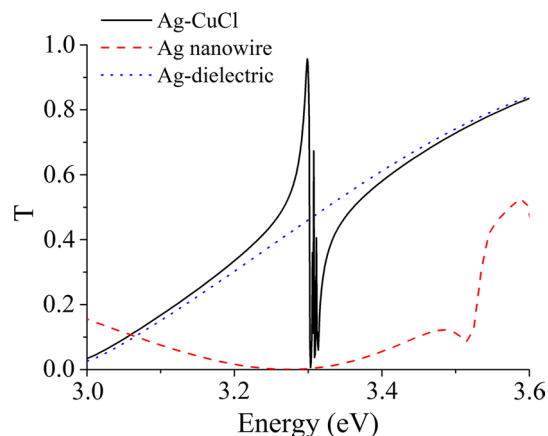
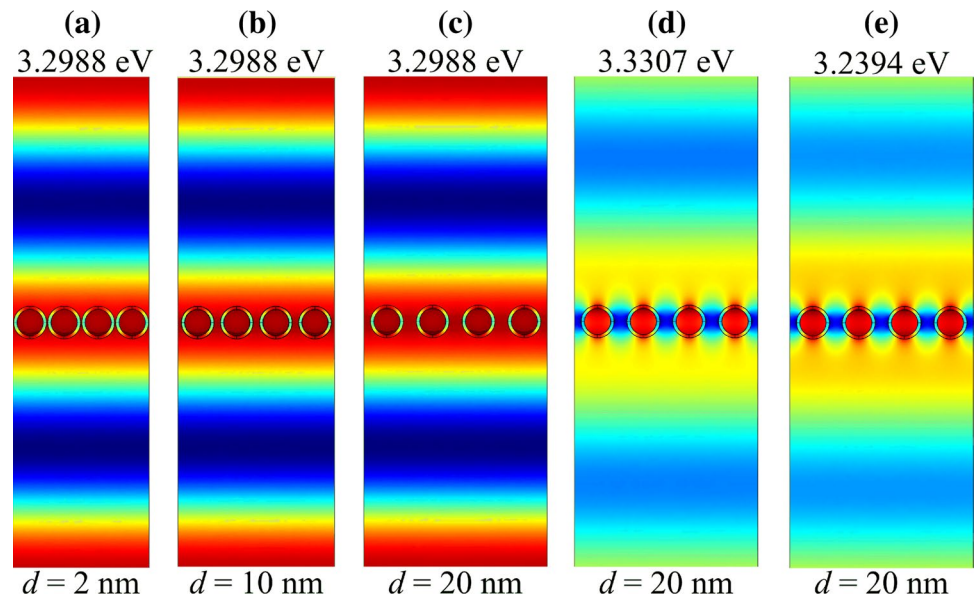


Fig. 6 Transmission spectra of the arrays of ACNWs, Ag nanowires, and Ag-dielectric nanowires

Figure 5b–d shows the transmission spectra of the ACNW arrays with $d = 2, 10,$ and 20 nm, respectively. In Fig. 5b, an extraordinary transmittance can be found at about 3.2988 eV, which accords with the location of the scattering dip in the ACNW. In Fig. 5c, d, the extraordinary transmittances of the ACNW arrays always locate at about 3.2988 eV. Thus, the extraordinary transmittance of the ACNW array does not depend on the distance between

Fig. 7 Electric field (E_x) distributions of the TE wave propagating through the ACNW arrays with **a** $d = 2$ nm, **b** $d = 10$ nm, and **c** $d = 20$ nm. Here, the calculation frequency is fixed at 3.2988 eV. Electric field (E_x) distributions of the TE wave propagating through the ACNW array with $d = 20$ nm at **d** 3.3307 eV and **e** 3.2394 eV



the two ACNWs. In addition, we also have calculated the transmission spectra of the Ag nanowire arrays. In Fig. 6, the solid, dashed, and dotted lines show the transmission spectra of the arrays of ACNWs, Ag nanowires, and Ag–dielectric nanowires, respectively. Here, the d value for the ACNW array is fixed at 2 nm. In the Ag nanowire array, the radius of the Ag nanowire and the d value are fixed at 20 and 7 nm, respectively. For the Ag–dielectric array, $r_1 = 20$ nm, $r_2 = 25$ nm, $\epsilon_2 = 5.59$, and $d = 2$ nm. It is obvious that the extraordinary transmittance only happens in the ACNW array, which arises from the plasmon–exciton coupling.

Figure 7a–c represents the visualizations of the TE wave propagating through the ACNW arrays with $d = 2, 10,$ and 20 nm, respectively. The frequency is fixed at 3.2988 eV. The three ACNW arrays are transparent at this frequency, and the d value does not affect the transmission of the TE wave. Therefore, the plasmon–exciton induced transparency in the ACNW array arises from the single ACNW, which should be a useful meta-atom for designing the metamaterials. Figure 7d, e shows the TE wave propagating through the ACNW array at 3.3307 ($\omega_{Ag|1}^e$) and 3.2394 eV ($\omega_{Ag|1}^l$), respectively. Here, d is fixed at 20 nm. At the two modes, the ACNW array becomes opaque because of the plasmon–exciton couplings in the ACNWs and the interactions between the adjacent nanowires.

In addition, we should indicate that the above results may have some changes for the finite-length nanowire. For the finite-length ACNW, if the length of the nanowire is much longer than the diameter, the influences of the two cross sections on the plasmon resonances and couplings are weak and can be neglected. However, when the length of the nanowire is comparable to the diameter, the effects of

the two cross sections on the plasmon resonances and couplings should be considered. Under this condition, as the incident polarization is parallel to the axis of the nanowire, the collective motions of the conduction electrons in the two cross sections will occur, and hence, another plasmon resonance mode will be found in the Ag nanowire. As the incident polarization is perpendicular to the axis of the nanowire, the localizations from the two cross sections also will affect the plasmon resonances in the Ag nanowire. Therefore, the corresponding plasmon–exciton couplings in the finite-length ACNWs should be different to those in the infinite-length ACNWs. We will further investigate the plasmon–exciton couplings in the finite-length ACNWs in our next work.

4 Conclusions

We have investigated the plasmon–exciton coupling properties of the ACNWs and associated arrays by using the scattering theory and the 2D-FEM. It is found with increasing the CuCl shell thickness that the $\omega_{Ag|1}$ mode can move through the ω_e mode. The Rabi splitting can occur in the ACNW. The strong coupling between the $\omega_{Ag|1}$ and ω_e modes leads to the hybridized $\omega_{Ag|1}^e$ and $\omega_{Ag|1}^l$ modes, which correspond to the antibonding and bonding between the $\omega_{Ag|1}$ and ω_e modes, respectively. The dispersion curves of the plexitonic modes in the ACNWs have been studied, and the obtained Rabi splitting energy is about 88 meV. Furthermore, the sharp ω_e peak interacts with the broad $\omega_{Ag|1}$ peak resulting in a deep dip in the scattering spectra of the ACNWs. As the TE wave propagates through the ACNW array, an extraordinary transmittance can be

observed at the scattering dip for the ACNW. This induced transparency does not depend on the distance between the two ACNWs, which arises from the single ACNW.

Acknowledgments This work was supported by the National Basic Research Program of China under Grant No. 2012CB921504, National Natural Science Foundation of China under Grant No. 11174113, Qing Lan Project of Jiangsu Province, and Senior Talent Foundation of Nanjing Normal University under Grant No. 2014102XGQ0189.

References

1. C.J. Murphy, Peer reviewed: optical sensing with quantum dots. *Anal. Chem.* **74**, 520A–526A (2002)
2. S.W. Bishnoi, C.J. Rozell, C.S. LeVin, M.K. Gheith, B.R. Johnson, D.H. Johnson, N.J. Halas, All-optical nanoscale pH meter. *Nano Lett.* **6**, 1687–1692 (2006)
3. A.O. Govorov, I. Carmeli, Hybrid structures composed of photo-synthetic system and metal nanoparticles: plasmon enhancement effect. *Nano Lett.* **7**, 620–625 (2007)
4. A.O. Govorov, G.W. Bryant, W. Zhang, T. Skeini, J. Lee, N.A. Kotov, J.M. Slocik, R.R. Naik, Exciton–plasmon interaction and hybrid excitons in semiconductor-metal nanoparticle assemblies. *Nano Lett.* **6**, 984–994 (2006)
5. M. Achermann, Exciton–plasmon interactions in metal–semiconductor nanostructures. *J. Phys. Chem. Lett.* **1**, 2837–2843 (2010)
6. F. Nagasawa, M. Takase, K. Murakoshi, Raman enhancement via polariton states produced by strong coupling between a localized surface plasmon and dye excitons at metal nanogaps. *J. Phys. Chem. Lett.* **5**, 14–19 (2014)
7. U. Kreibig, M. Vollmer, *Optical Properties of Metal Clusters* (Springer, New York, 1995)
8. A. Panahpour, Y. Silani, M. Farrokhanian, A.V. Lavrinenko, H. Latifi, Coupled plasmon–exciton induced transparency and slow light in plexcitonic metamaterials. *J. Opt. Soc. Am. B* **29**, 2297–2308 (2012)
9. B.J. Lawrie, K.W. Kim, D.P. Norton, R.F. Haglund, Plasmon–exciton hybridization in ZnO quantum-well Al nanodisc heterostructures. *Nano Lett.* **12**, 6152–6157 (2012)
10. C. Ayala-Orozco, J.G. Liu, M.W. Knight, Y.M. Wang, J.K. Day, P. Nordlander, N.J. Halas, Fluorescence enhancement of molecules inside a gold nanomatryoshka. *Nano Lett.* **14**, 2926–2933 (2014)
11. J.T. Zhang, Y. Tang, K. Lee, M. Ouyang, Tailoring light–matter–spin interactions in colloidal hetero-nanostructures. *Nature* **466**, 91–95 (2010)
12. A. Hatef, S.M. Sadeghi, S. Fortin-Deschênes, E. Boulais, M. Meunier, Coherently-enabled environmental control of optics and energy transfer pathways of hybrid quantum dot-metallic nanoparticle systems. *Opt. Express* **21**, 5643–5653 (2013)
13. S. Lambright, E. Butaeva, N. Razgoniaeva, T. Hopkins, B. Smith, D. Perera, J. Corbin, E. Khon, R. Thomas, P. Moroz, A. Mereshchenko, A. Tarnovsky, M. Zamkov, Enhanced lifetime of excitons in nonepitaxial Au/CdS core/shell nanocrystals. *ACS Nano* **8**, 352–361 (2014)
14. J. Dintinger, S. Klein, F. Bustos, W.L. Barnes, T.W. Ebbesen, Strong coupling between surface plasmon-polaritons and organic molecules in subwavelength hole arrays. *Phys. Rev. B* **71**, 035424 (2005)
15. P. Vasa, R. Pomraenke, S. Schwieger, Y.I. Mazur, V. Kunets, P. Srinivasan, E. Johnson, J.E. Kihm, D.S. Kim, E. Runge, G. Salamo, C. Lienau, Coherent exciton–surface-plasmon-polariton interaction in hybrid metal–semiconductor nanostructures. *Phys. Rev. Lett.* **101**, 116801 (2008)
16. W. Wang, P. Vasa, R. Pomraenke, R. Vogelgesang, A. De Sio, E. Sommer, M. Maiuri, C. Manzoni, G. Cerullo, C. Lienau, Interplay between strong coupling and radiative damping of excitons and surface plasmon polaritons in hybrid nanostructures. *ACS Nano* **8**, 1056–1064 (2014)
17. G.A. Wurtz, P.R. Evans, W. Hendren, R. Atkinson, W. Dickson, R.J. Pollard, A.V. Zayats, W. Harrison, C. Bower, Molecular plasmonics with tunable exciton-plasmon coupling strength in J-aggregate hybridized Au nanorod assemblies. *Nano Lett.* **7**, 1297–1303 (2007)
18. A.E. Schlather, N. Large, A.S. Urban, P. Nordlander, N.J. Halas, Near-field mediated plexcitonic coupling and giant Rabi splitting in individual metallic dimers. *Nano Lett.* **13**, 3281–3286 (2013)
19. N.T. Fofang, T.H. Park, O. Neumann, N.A. Mirin, P. Nordlander, N.J. Halas, Plexcitonic nanoparticles: plasmon–exciton coupling in nanoshell–J-aggregate complexes. *Nano Lett.* **8**, 3481–3487 (2008)
20. N.T. Fofang, N.K. Grady, Z.Y. Fan, A.O. Govorov, N.J. Halas, Plexciton dynamics: exciton plasmon coupling in a J-aggregate Au nanoshell complex provides a mechanism for nonlinearity. *Nano Lett.* **11**, 1556–1560 (2011)
21. S. Savasta, R. Saija, A. Ridolfo, O. Di Stefano, P. Denti, F. Borghese, Nanopolaritons: vacuum Rabi splitting with a single quantum dot in the center of a dimer nanoantenna. *ACS Nano* **4**, 6369–6376 (2010)
22. A. Manjavacas, F.J. García de Abajo, P. Nordlander, Quantum plexcitonics: strongly interacting plasmons and excitons. *Nano Lett.* **11**, 2318–2323 (2011)
23. D.C. Marinica, H. Lourenco-Martins, J. Aizpurua, A.G. Borisov, Plexciton quenching by resonant electron transfer from quantum emitter to metallic nanoantenna. *Nano Lett.* **13**, 5972–5978 (2013)
24. J.T. Manassah, Electrodynamics of semiconductor-coated noble metal nanoshells. *Phys. Rev. A* **87**, 053845 (2013)
25. V. Yannopapas, N.V. Vitanov, Photoexcitation-induced magnetism in arrays of semiconductor nanoparticles with a strong excitonic oscillator strength. *Phys. Rev. B* **74**, 193304 (2006)
26. D.J. Wu, Y. Cheng, X.W. Wu, X.J. Liu, Exciton–plasmon couplings in plexcitonic CuCl–Ag nanoshells: Rabi splitting and induced transparency. *J. Opt. Soc. Am. B* **31**, 2273–2277 (2014)
27. Y. Fedutik, V. Temnov, U. Woggon, E. Ustinovich, M. Artemyev, Exciton–plasmon interaction in a composite metal–insulator–semiconductor nanowire system. *J. Am. Chem. Soc.* **129**, 14939–14945 (2007)
28. C.H. Cho, C.O. Aspetti, M.E. Turk, J.M. Kikkawa, S.W. Nam, R. Agarwal, Tailoring hot-exciton emission and lifetimes in semiconducting nanowires via whispering-gallery nanocavity plasmons. *Nat. Mater.* **10**, 669–675 (2011)
29. J.Y. Yan, Optical properties of excitons in metal–insulator–semiconductor nanowires. *Opt. Express* **21**, 25607–25618 (2013)
30. R.D. Averitt, S.L. Westcott, N.J. Halas, Linear optical properties of gold nanoshells. *J. Opt. Soc. Am. B* **16**, 1824–1832 (1999)
31. M. Artoni, G. La Rocca, F. Bassani, Resonantly absorbing one-dimensional photonic crystals. *Phys. Rev. E* **72**, 046604 (2005)
32. D.J. Wu, X.J. Liu, B. Li, Localized surface plasmon resonance properties of two-layered gold nanowire: effects of geometry, incidence angle and polarization. *J. Appl. Phys.* **109**, 083540 (2011)
33. W. Liu, A.E. Miroshnichenko, R.F. Oulton, D.N. Neshev, O. Hess, Y.S. Kivshar, Scattering of core-shell nanowires with the interference of electric and magnetic resonances. *Opt. Lett.* **38**, 2621–2623 (2013)

34. J. Jin, *The finite element method in electromagnetics* (Wiley, New York, 1993)
35. M. Wang, M. Cao, X. Chen, N. Gu, Subradiant plasmon modes in multilayer metal–dielectric nanoshells. *J. Phys. Chem. C* **115**, 20920–20925 (2011)
36. D.J. Wu, S.M. Jiang, X.J. Liu, Fano-like resonances in asymmetric homodimer of gold elliptical nanowires. *J. Phys. Chem. C* **116**, 13745–13748 (2012)
37. D.J. Wu, S.M. Jiang, Y. Cheng, X.J. Liu, Fano-like resonance in symmetry-broken gold nanotube dimer. *Opt. Express* **20**, 26559–26567 (2012)
38. Y.B. Zheng, B.K. Juluri, L.L. Jensen, D. Ahmed, M.Q. Lu, L. Jensen, T.J. Huang, Dynamical tuning of plasmon–exciton coupling in arrays of nanodisk-J-aggregate complexes. *Adv. Mater.* **22**, 3603–3607 (2010)